

Highly Sensitive and Self Powered Ultraviolet Photo Detector based on ZnO Nanorods Coated with TiO₂

Shashi Pandey¹, Alok Shukla^{2*}, Anurag Tripathi¹

¹*Department of Electrical Engineering IET Lucknow, Uttar Pradesh 226021, India*

²*Department of Physics, Indian Institute of Technology Bombay, Powai, Mumbai 400076, India*

Abstract

Nanorods (NRs) of crystalline ZnO coated with thin layers of TiO₂ (ZnO@TiO₂) were fabricated with the help of spin coating technique followed by hydrothermal method. Scanning electron microscopy (SEM) and X-ray diffraction analysis confirms the morphology and structural stability of as-prepared NRs. The optical band gaps of the NRs were estimated, and a clear blue-shift towards the UV region has been detected. When UV light falls on as-prepared device (i.e., in the “ON” state), a significant increase in photocurrent (I_{UV}) at zero voltage supply was observed from 6 μ A to 17 μ A, while in the “OFF” state, the dark current (I_{dark}), increases from 0.08 μ A to 0.6 μ A with ZnO@TiO₂ NRs as compared to bare ZnO NRs respectively. Responsivity and detectivity of TiO₂ coated ZnO NRs based device found maximum in UV region unlike bare ZnO NRs. Enhanced photocurrent achieved by the growth of TiO₂ layers on ZnO NRs is 250 μ A as compared to bare ZnO NRs for which it is 35 μ A at 10V voltage supply under the ultraviolet irradiation (illumination intensity of 1 mW/cm²). Furthermore, theoretical calculations have been performed using the first-principles density-functional theory to understand the effects of heterostructure NRs on the electronic and optical properties of TiO₂ coated ZnO.

Keywords: *Zinc Oxide, Titanium Dioxide, Nanorods, hydrothermal method, Spin coating, Photo detector.*

Email: 2512@ietlucknow.ac.in, shukla@phy.iitb.ac.in, anurag.tripathi@ietlucknow.ac.in

**corresponding author*

Introduction

Ultraviolet photo detection has many applications in the field of optical imaging, optoelectronic circuits, military surveillance, air quality monitoring, and even in space communication [1]–[4]. Conventional photo detectors based on materials such as silicon, germanium, gallium arsenide, and silicon carbide, etc. become expensive because they require high temperature conditions for device fabrication, as well as visible light filters. Therefore, the invention of fast, sensitive, direct UV detectors, that are easy to synthesize, is important. For high UV sensitivity, we need materials that are transparent in the lower-energy region of the spectrum, and have strong optical response in the UV region. Devices based on several semiconducting oxides are very useful for the purpose because of their environment friendly nature, non-toxic character, large band-gap leading to high UV sensitivity, low cost, and excellent thermal stability. The sensitivity to the UV light in these materials can be further tuned by constructing nanostructures of different shapes and sizes, and also by managing oxygen adsorption and native defects [5]–[7].

In this work we have explored the optical response of nano-rods (NRs) of a transition metal oxide, namely, crystalline ZnO, coated with thin layers of TiO₂ (ZnO@TiO₂). Pure ZnO is not a good candidate for such devices because it has inherent deep levels and surface defects [8] which enhance undesirable photocurrent leading to low sensitivity and switching stability during device operation. Recently, a few groups studied the synthesis and optical response of TiO₂ and ZnO-based nanocomposites, with the purpose of demonstrating improved device performance [9], [10], as compared to bare ZnO nanostructures. TiO₂ has a wide range of applications [8], [11]–[13] such as in photo detectors, gas sensors, and thermal catalysis. In several studies, enhancement in UV photo detection properties of ZnO, by changing its morphology, was pursued [14]–[19]. On the other hand, many works have suggested that doping of different materials in ZnO can improve its optoelectronic and photoconductive properties [3], [20]–[22]. Because of its excellent thermal and photochemical stability, TiO₂ has been investigated as a candidate for enhancing the optoelectronic properties of nanocomposite devices [23]. In order to increase the sensitivity of photodetectors, researchers have focused more on the coupling of semiconductors, particularly a heterojunction based on two types of semiconductors with differing energy band structures [24]. As a result of the coupling of various energy level structures, TiO₂ and ZnO are strong candidates to produce a heterostructure with improved characteristics compared to those of either material alone. Wang et

al [24] reported that ZnO@TiO₂ nanostructures also play an important role in dye-sensitized solar cells applications. ZnO is a well-known n-type semiconductor due to the presence of native defects [25]–[27], as a result of which electrons (i.e., its majority charge carriers) already exist in its conduction band at the room temperature[28]. As a result of this, while measuring the photocurrent; one sees a drop in the photocurrent in the UV “OFF” state of the bare ZnO samples. However, in the UV “ON” state, the photocurrent increases because of the photon-induced promotion of the valence band electrons to the conduction band in bare ZnO[28], [29]. As far as ZnO@TiO₂ NRs are concerned, because of the high reactivity of anatase TiO₂, a significant O₂ desorption takes place, thus freeing up electrons, leading to a large rise in the photocurrent in the UV “ON” state, as compared to the bare ZnO NRs [16], [18], [19], [24]. Hence, this work will improve the understanding of heterostructures based on semiconducting oxides, which leads to enhance the optoelectronic properties of devices.

Experimental Procedure

A. Synthesis and Characterization of ZnO@TiO₂ Nano rods

Firstly, cleaning of ITO substrate was done using acetone and methanol or IPA. ITO substrate cleaned with firstly under acetone and then put in methanol quickly before it dries after taking out from acetone. Then the mixture of zinc acetate dehydrates and ethanolamines (with ratio 1:2) were dissolved in 25 mL 2-methoxy ethanol. Next, the prepared solution was stirred at 50 °C for 1 hour, and then spin-coated with 2500 rpm for 1 min onto indium-tin oxide (ITO) glass substrates. The resultant sample was further heated at 350 °C for 6 hours to obtain ZnO NRs on the ITO substrate. Next, the prepared NRs of ZnO were placed inside an autoclave, which contained diethylenetriamine, isopropyl alcohol, and a titanium (IV) isopropoxide. Autoclave, containing the mixture, was given a heat treatment (200 °C for 12 hours), after which the as-prepared sample was smoothly rinsed with ethanol and acetone at the room temperature. Finally, the rinsed sample was annealed at 450 °C for 6 hours to confirm the deposition (i.e. coating) of crystalline phases of TiO₂ on ZnO NRs. For structural and morphological characterizations, Zeiss Supra-55 field emission scanning electron microscope (FESEM) was used. In order to examine the structural phase purity of the prepared samples, the powder x-ray diffraction (XRD) experiments were carried out on Bruker D8 diffractometer equipped with Cu target having LYNXEYE detector. The high temperature x-ray diffraction measurements were performed to

confirm the structural phases of the prepared samples. The optical band gap of prepared sample has been measured using diffuse reflectivity measurements. These measurements have been performed in the 200 nm to 800 nm wavelength range using Perkin Elmer LAMBDA 950 UV-Vis-NIR Spectrophotometer. For device fabrication Ag (thickness 50 nm) has been deposited as an electrode using thermal evaporation. Shadow masking was used to keep the width to 1 mm and the distance between the Ag electrodes (channel length) to 100 μm . Electrical characterizations were performed by Keithley 2612A source meter.

B. Computational details

The first-principles calculations to support the experimental results were performed within the framework of plane-wave density-functional theory (PW-DFT) [30], [31] as implemented in Vienna ab-initio simulation package (VASP)[32], [33]. To match our calculated bandgap with the experimental results, the generalized gradient approximation coupled with the Hubbard U (GGA+U) level of theory was used [34], [35]. We performed calculations both on the bare ZnO NRs, and the ZnO@TiO₂ NRs, and the super cells used for the two systems are shown in Fig. 1. To model the bare NRs, we used a one-dimensional super cell of dimension 12x1x1 (see Fig. 1(a)) of bulk ZnO, while for simulating ZnO@TiO₂ NRs, we added one-unit cell of the anatase phase of TiO₂ containing twelve atoms (4 Ti and 8 O) on one of the ends of the ZnO super cell. Furthermore, to model the finite size of the NRs, 10 Å of vacuum was used in two directions, as shown in Fig. 1. One can ask as to why did we model ZnO@TiO₂ NRs by attaching a unit cell of TiO₂ only on one tip of the bare NRs, and not on the second tip and other places? The reason behind this choice is that the SEM images presented in the next section clearly show that the ZnO@TiO₂ NRs have TiO₂ attached only on one tip of the bare NRs, and nowhere else. As far as the optimized geometries of the two types of NRs presented in Fig. 1 are concerned: (a) bare NRs were found to be 39.28 Å long, with a diameter of 5.20 Å (Fig. 1(a)), and (b) the total length

of ZnO@TiO₂ NRs is approximately 43.01 Å, with the diameter on the ZnO side of around 5.20 Å, and on the TiO₂ side 3.73 Å (Fig. 1(b)).

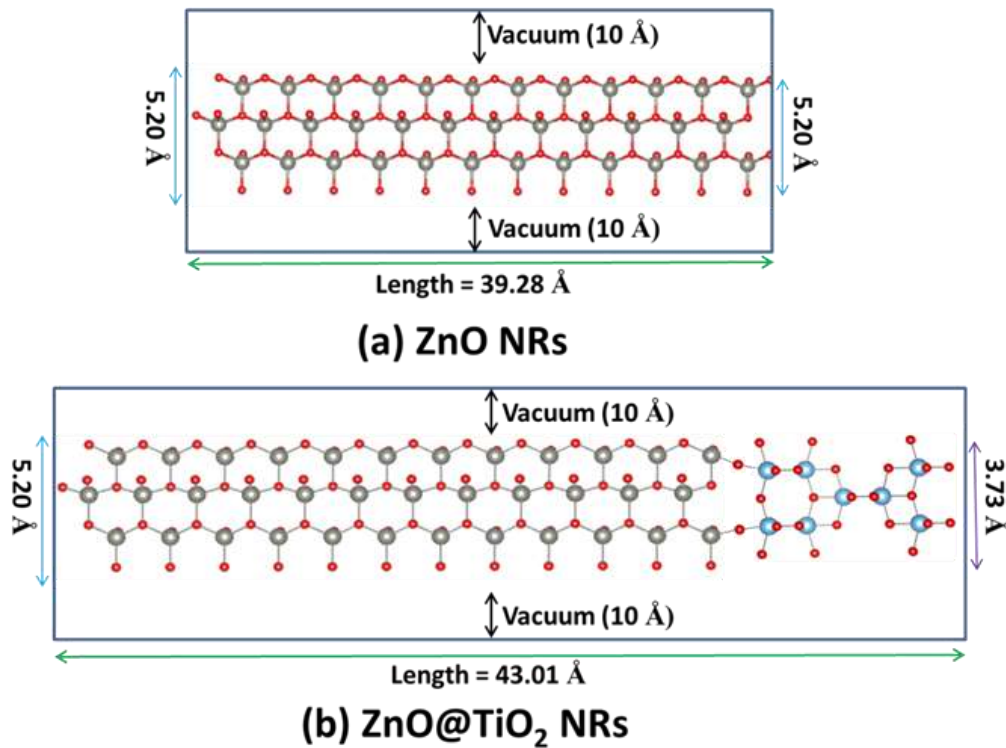


FIGURE 1: Structural Images of (a) bare ZnO having 12x1x1 supercell and (b) composite of ZnO having supercell 12x1x1 along with TiO₂ with single unit cell. Blue and red color indicates Zn, Ti and O atoms respectively.

Results and Discussion

Figure 2(a) shows the SEM image of the as-prepared ZnO@TiO₂ on ITO glass substrate. Firstly, the ZnO NRs have been deposited on ITO glass substrate using spin coating method (see Figure 2(b)). Figure 2(b) shows the vertical orientation of ZnO NRs (top view). Deposition of TiO₂ on ZnO NRs was done using the hydrothermal process, and as-prepared TiO₂ nanocomposites on ZnO[37] are also shown in Figure 2(a) and 2(b). The average length and diameter of the NRs were around 1.80 μm and 150 nm with particle size 3-23.2 nm. From the top view of SEM image, TiO₂ has been deposited only on the exposed tips of ZnO NRs (see figure 2(b)), The nanostructures (NRs) are typically about 1 μm in length and 150–200 nm in diameter. Hence, the SEM analysis confirms the fabrication of ZnO@TiO₂ NRs.

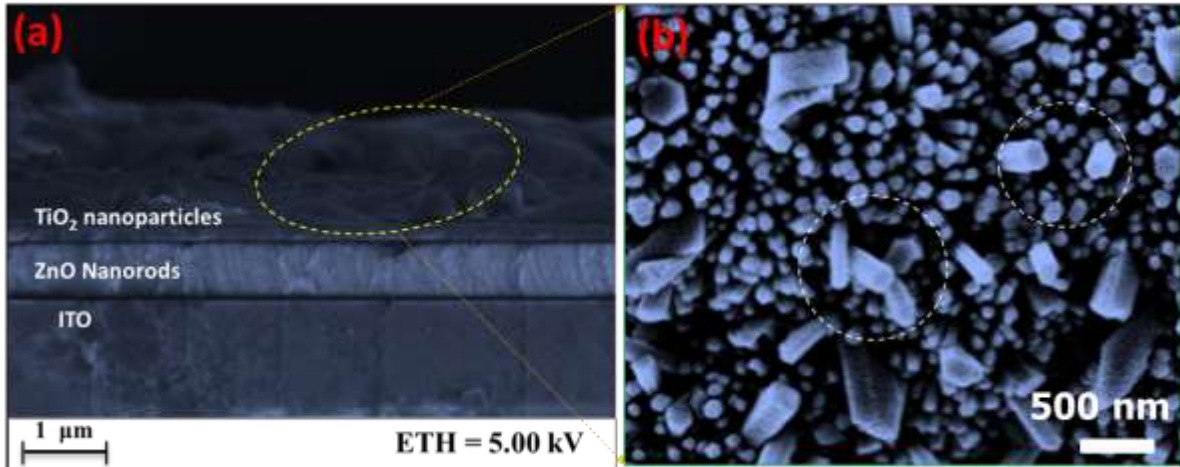


FIGURE 2: FESEM images of (a) deposited TiO₂ on ZnO NRs, (b) shows enlarged view (yellow color) of deposited TiO₂ nanoparticles on ZnO NRs.

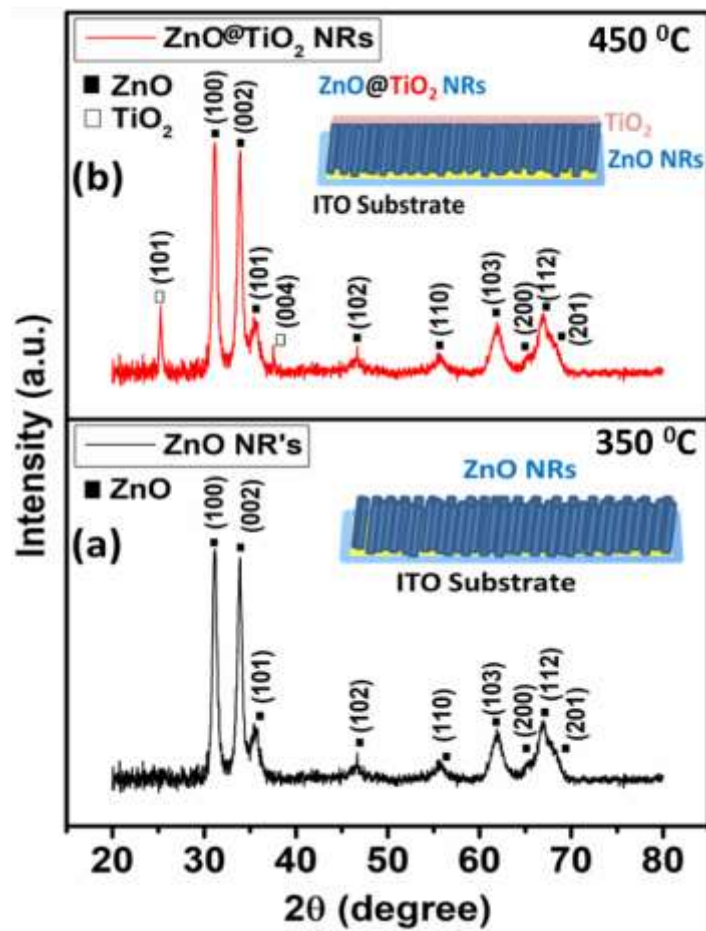


FIGURE 3: X-Ray diffraction patterns of as-prepared ZnO and ZnO@TiO₂ NRs.

To probe the structural stability of our prepared ZnO@TiO₂ nanocomposites, we have performed X-ray diffraction analysis (see Figure-3). X-ray diffraction patterns of the as-prepared ZnO NRs have been shown in figure-3(a) and indexing of all the diffraction peaks confirms the hexagonal wurtzite structure of ZnO[38], [39]. The x-ray diffraction pattern of ZnO@TiO₂ is shown in Figure 3(b) and additional peaks corresponding to (101) and (004) planes of the anatase phase of TiO₂ are clearly observed. These coupled with the SEM images further confirm the formation of the ZnO@TiO₂ composite NRs, with the TiO₂ deposited on the tips. We have probed the optical absorption for bare ZnO NRs and TiO₂ coated ZnO NRs using diffuse reflectance spectroscopy. The spectra obtained from DRS is converted into equivalent absorption spectra through Kubelka–Munk equation [8,13],

$$F(R_{\infty}) = \frac{(1-R_{\infty})^2}{2R_{\infty}}, \quad (i)$$

Where $F(R_{\infty})$ is the Kubelka–Munk function, $R_{\infty} = R_{sample}/R_{standard}$. The Kubelka–Munk function can be related (proportional) to the absorption coefficient (α) as-

$$F(R_{\infty}) \propto \alpha \propto \frac{(h\nu - E_g)^{1/n}}{h\nu}, \quad (ii)$$

In order to calculate the E_g , the obtained absorption coefficient is converted in to Tauc equation [13] and plotted in figure 4.

$$(\alpha h\nu)^n = A(h\nu - E_g), \quad (iii)$$

Here in equation (iii) ‘n’ has the value of 2 for direct bandgap transitions (used for ZnO bare NRs), while n is equal to 1/2 for an indirect transition (used for ZnO@TiO₂ NRs) [13]. To see the change in the optical band gap of deposited ZnO[8], [16], [17], and ZnO@TiO₂ NRs, optical absorption measurements have been carried out in the range 300 nm to 900 nm. It is well known that bulk ZnO has a band gap of 3.3 eV, while our measured value of the optical gap of ZnO NRs is 3.46 (see Fig. 4). Clearly, band gap increases in the NR phase, as compared to the bulk [40], [41]. Our measured optical gap of as prepared ZnO@TiO₂ NRs further increases to 3.56 eV (see Fig. 4), which is closer to the UV range. This increase can clearly be attributed to the presence of TiO₂ in the sample.

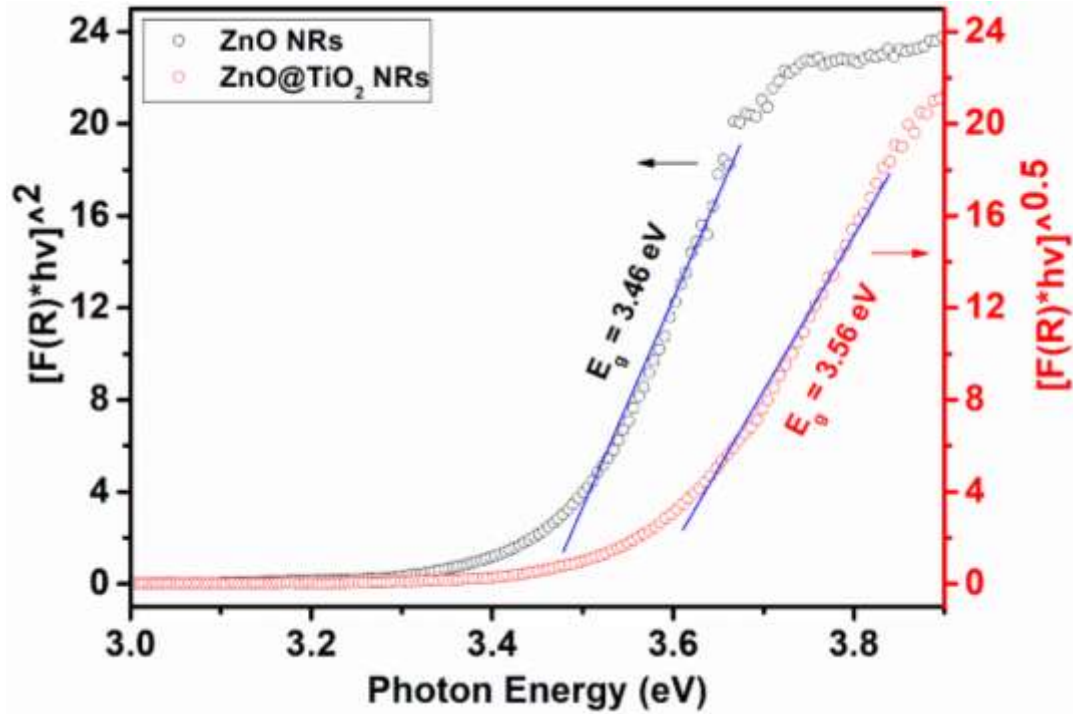


FIGURE 4: Measured optical absorption spectra of ZnO and ZnO@TiO₂ NRs.

To verify the experimental band gap of nanocomposites of ZnO and TiO₂, systematic first-principles DFT calculations of total density of states (TDOS)[42] and optical absorption spectra have been performed. Figure 5 show TDOS of bare ZnO NRs with an electronic band gap of 3.46 eV calculated using the GGA+U method [43] with U=4.3 eV (at Zn sites), while the inset shows the optical absorption spectrum obtained from the same calculations. We have performed similar calculations for ZnO@TiO₂ NRs, and observed a clear blue shift in band gap as compared to bare ZnO NRs. In Fig. 6 we show TDOS of ZnO@TiO₂ NRs with an electronic band gap of 3.58 eV obtained the using the GGA+U calculations with U=4.3 eV at the Zn sites and U=5.6 eV at the Ti sites, along with the computed optical absorption spectrum shown in the inset. Very good quantitative agreement between the theoretically computed band gaps with the experimentally measured ones indicates that our choice of U parameters in the GGA+U calculations is correct (see Figs. 4, 5 and 6).

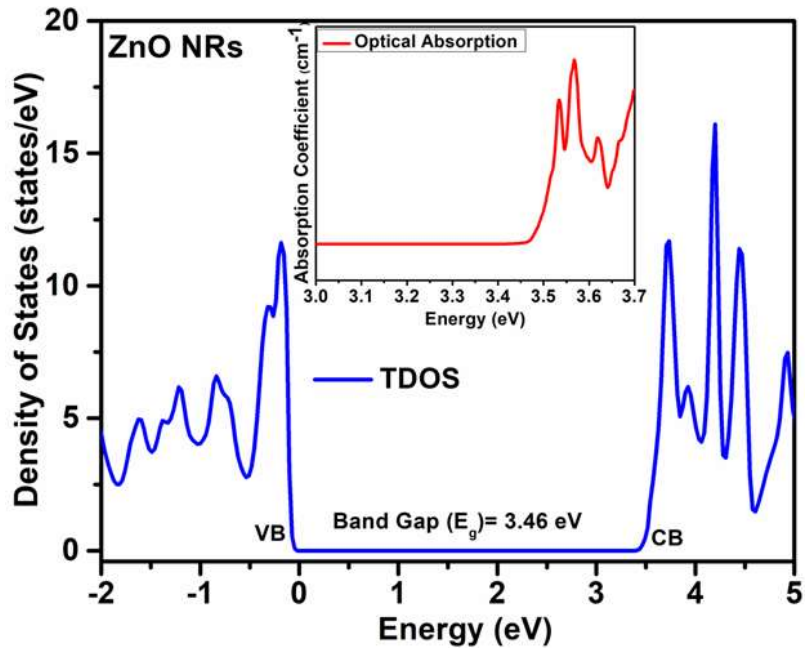


FIGURE 5: TDOS of ZnO NRs exhibits an electronic band gap of 3.46 eV obtained from the GGA+ U calculations ($U=4.3$ eV). The inset shows the calculated optical absorption spectrum of bare ZnO NRs.

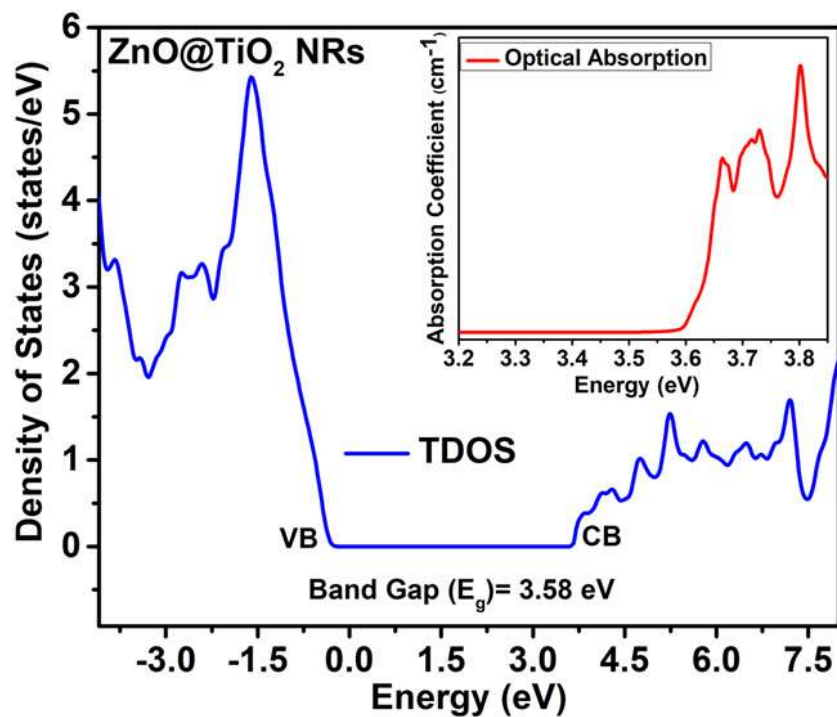


FIGURE 6: TDOS of ZnO@TiO₂ NRs shows electronic band gap of 3.58 eV using GGA+ U calculations ($U=4.3$ eV for Zn and $U=5.6$ eV for Ti). The inset shows simulated optical absorption spectrum of ZnO@TiO₂ NRs.

The measurement setups for photocurrent spectra for ZnO NRs and ZnO@TiO₂ are shown in Figs. 7(a) and 7(b), respectively. Before performing the measurements, first we heated the prepared device up to a temperature of 300⁰C for 8 hours to avoid moisture, and then kept it in dark on vacuum desiccator for several hours to reach the equilibrium condition. I-V characteristics of ZnO NRs and ZnO@TiO₂ NRs measured using a UV lamp (with wavelength 365 nm) have been plotted in Figs.-7(c) and 7 (d), and it is clearly observed that with the increase in the voltage, the device current also increases for both cases. When UV is “ON”, the device current increases sharply, while for UV “OFF”, the increase in the current with the applied voltage is quite negligible. On comparing the I-V characteristics of bare ZnO NRs and ZnO@TiO₂ NRs (Figs.- 7(c) and 7(d)), we conclude that the TiO₂ coated on ZnO NRs enhances the value of the current with applied voltages. This result indicates that bare ZnO NRs as well as ZnO@TiO₂ NRs are highly UV sensitive; however, the photoelectric response of ZnO@TiO₂ NRs is much more intense. Insets (i) and (ii) of Figs. 7(c) and 7(d) respectively show that there are still small amounts of charge carriers inside the device at V=0, irrespective of whether the UV light is “ON” or “OFF”.

To determine the performance of device, responsivity, $R = (I_{UV}/I_P)$ [19], is an important parameter where, I_P is the incident power and I_{UV} is the maximum current under UV irradiation. From Fig. 8 (a) and 8 (b) it is clearly seen that responsivity of our device is maximum in UV region while it is decreasing in visible region. Detectivity ($D = 1/NEP_B$) [19] has been depicted in Fig. 8(a) and 8(b), and peak value reached at 1.8×10^{14} (at ~ 450 nm) and 6.4×10^{14} Hz^{1/2}/W (at 380 nm) for bare ZnO NRs and TiO₂ coated ZnO NRs respectively. It is clearly seen that in case of TiO₂ coated ZnO NRs shows enhancement in responsivity and detectivity both as compared to bare ZnO NRs.

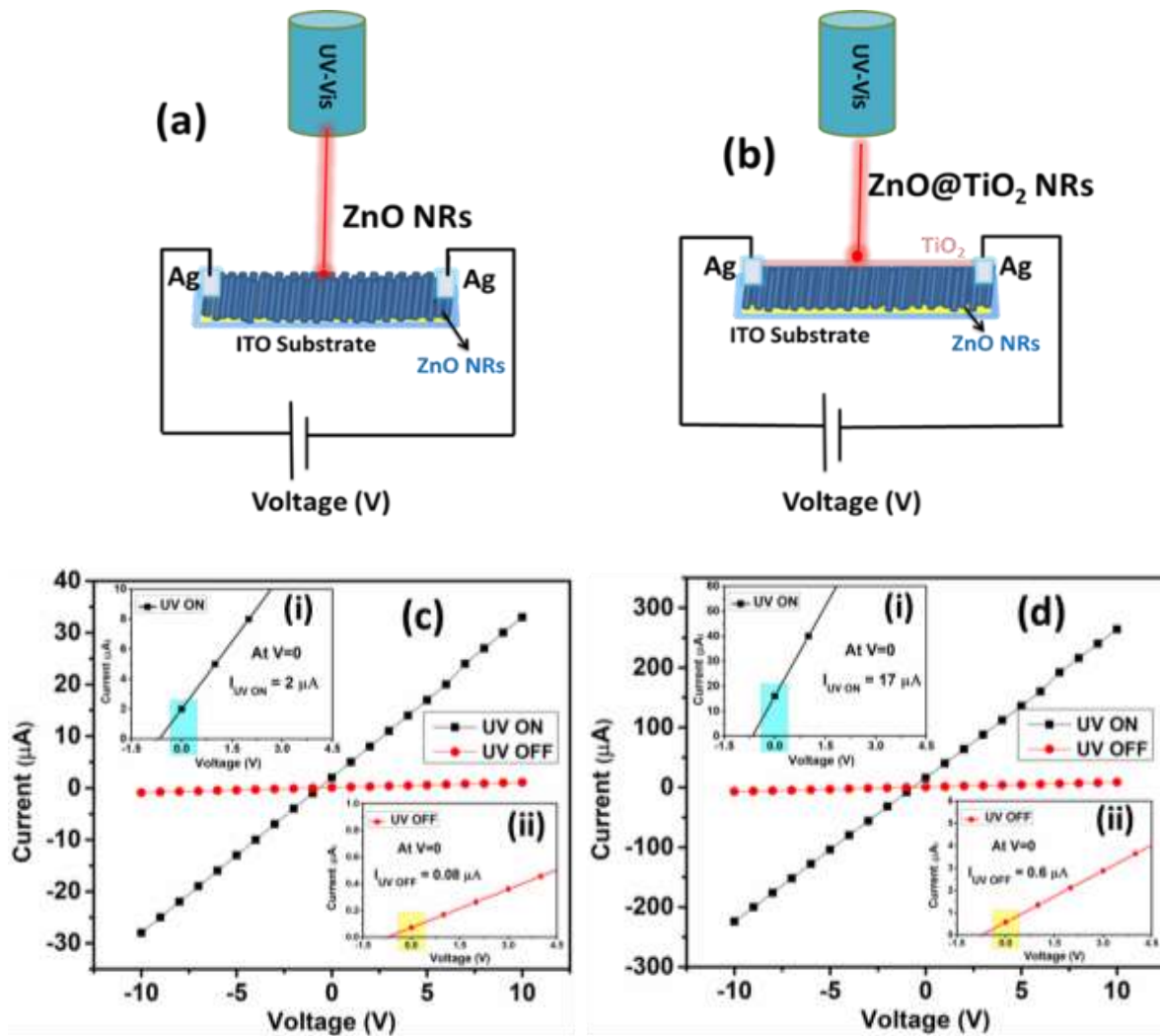


Figure 7: (a)-(b) Schematic of measurement setup for as prepared composite NRs using semiconducting oxides on ITO glass substrate (mechanism of producing photocurrent with applied field). Current-voltage characteristic of (c) ZnO NRs and (d) ZnO@TiO₂ NRs in presence of UV light, while insets of figures (c) & (d) show enlarged views of I-V characteristics.

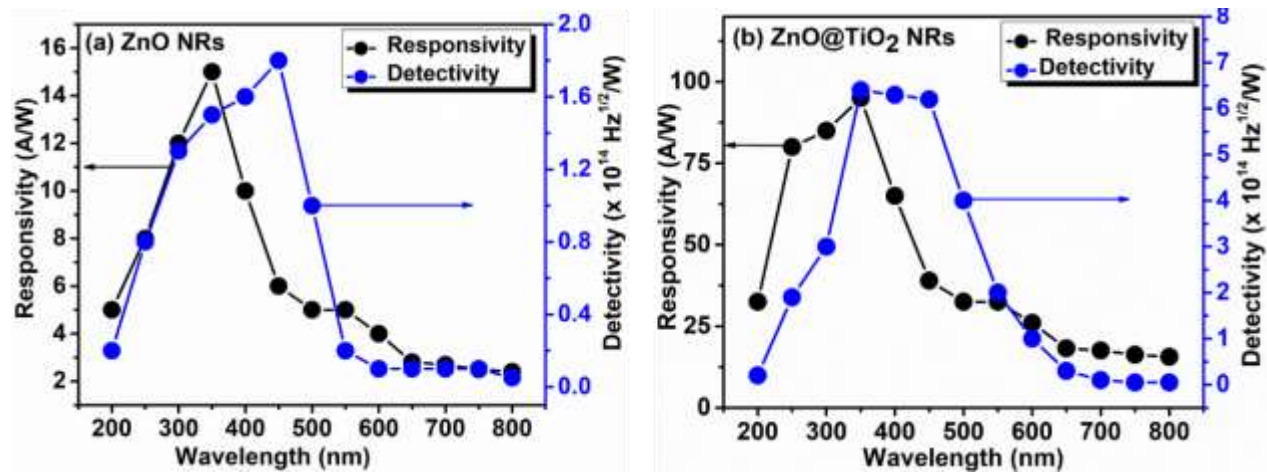


Figure 8: Responsivity and Detectivity of (a) bare ZnO and (b) TiO₂ coated ZnO NRs at different wavelengths.

In order to probe the stability of our devices, UV photocurrents of bare ZnO NRs and ZnO@TiO₂ NRs, at a constant bias voltage of 5 V, were measured under ambient conditions. For the purpose, the photons of wave lengths in the range 250nm - 750nm were alternatively switched “ON” and “OFF” for 10 minute each, and the results of our measurements are shown in Figs. 9 (a) and 9(b). This growth and decay of current can be used to sense UV as well as visible wavelengths. Interestingly, it is found that in case of visible light, photo current response is very low while in case of UV light photocurrent response increases ten times for prepared device. Cycles are similar and repeatable in nature, thus, confirming the reliability of both types of devices. Increase in the photocurrent under UV light is due to the promotion of a large number of electrons from the valence band to the conduction band because the photon energy exceeds the band gaps of our prepared devices. However, photons of larger wave lengths, i.e., those in the visible range, do not have sufficient energy to transfer the electrons from the valence to the conduction band, leading to considerable drop in the number of charge carriers, and, thus, the photocurrent. The photocurrent in the visible region is mainly because of the charge carriers generated due to native defects and impurities in the devices. Native defects such vacancies, self-interstitials, and anti-sites are inescapable during the synthesis of crystal lattices and have a significant impact on the performance of semiconducting oxide-based devices [42,44-47]. Significant changes in device performance, such as electronic bandgap, photocurrent, response time, etc., can be seen with a nominal change in defect concentration. This photocurrent detected in the visible area may be caused by the intrinsic oxygen deficiency found mostly in semiconducting oxides-based devices.

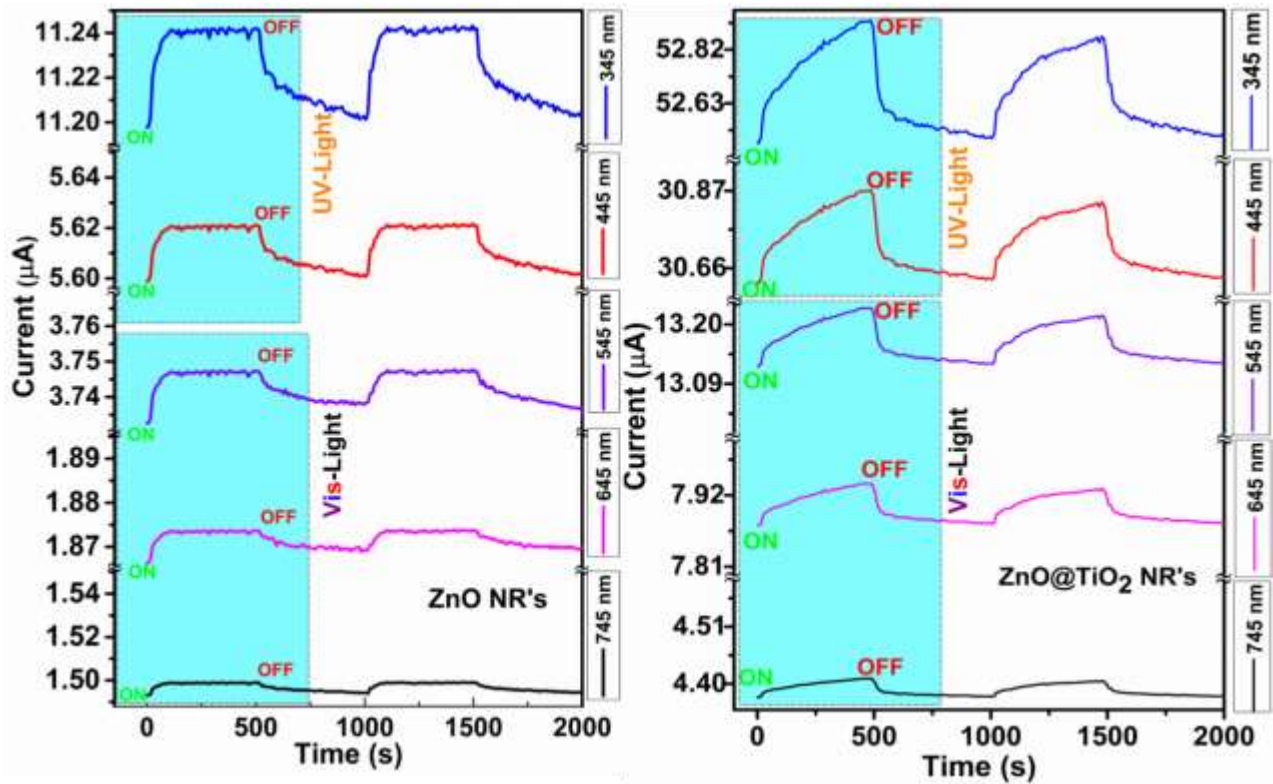


FIGURE 9: Photocurrent response of (a) ZnO NRs and (b) ZnO@TiO₂ NRs. In both case photocurrent response is maximum with UV light, while photocurrent decreases with increase in wavelength (i.e. for Visible light).

From Figs. 7, 8 and 9 it is obvious that ZnO@TiO₂ NRs has a significantly larger photocurrent response as compared to bare ZnO NRs, with a many-fold enhancement of current in the UV region. In order to systematically investigate the photo-response of the two types of devices as a function of the wavelength of the incident light, we performed measurements of the photocurrents of as prepared bare ZnO and ZnO@TiO₂ NRs by varying the wavelength and the results are presented in Fig. 10. From the figure it is obvious that: (a) in the entire region of wavelength probed in our experiment, the photocurrents measured in ZnO@TiO₂ NRs based devices is larger than that of ZnO NR based devices, and (b) the difference in two responses becomes large with the decreasing wavelengths, and for the shortest wavelength the photocurrent in the ZnO@TiO₂ NRs devices (53 µA) is almost five times of that in the bare ZnO devices (11.24 µA). Hence it is clearly seen that with coating of TiO₂ on ZnO NRs not only increases the photocurrent but also increases photosensitivity and switching stability of prepared device as compare to bare ZnO NRs.

Photocurrent in the visible region is mainly because of the charge carriers generated due to native defects and impurities in the devices. From the figure it is obvious that: (a) in the entire region of wavelength probed in our experiment, the photocurrents measured in ZnO@TiO₂ NRs based devices is larger than that of ZnO NR based devices, and (b) the difference in two responses becomes large with the decreasing wavelengths, and for the shortest wavelength the photocurrent in the ZnO@TiO₂ NRs devices (53 μ A) is almost five times of that in the bare ZnO devices (11.24 μ A). Hence it is clearly seen that with coating of TiO₂ on ZnO NRs not only increases the photocurrent but also increases photosensitivity and switching stability of prepared device as compare to bare ZnO NRs.

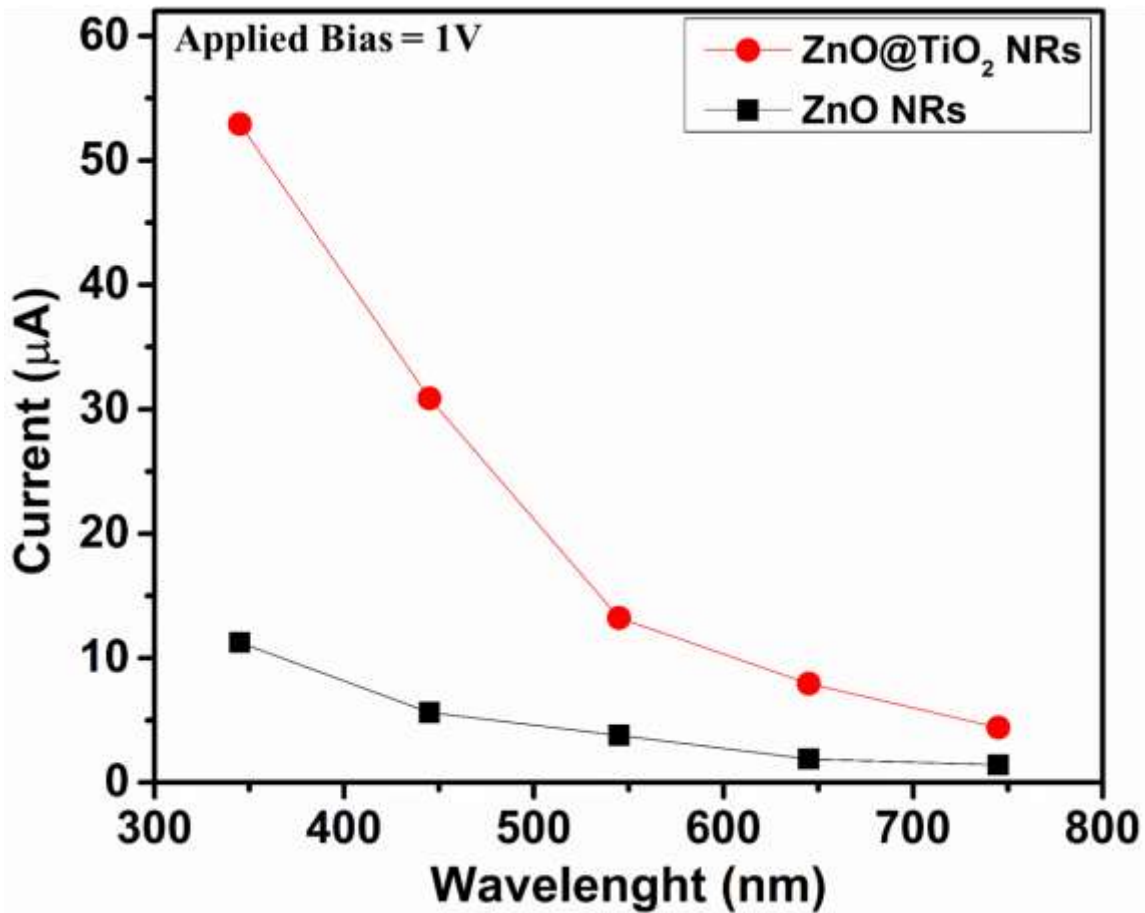


FIGURE 10: *Current vs wavelength plot shows photocurrent decreases with increase in the wavelength of the incident light on bare ZnO NRs and ZnO@TiO₂ NRs with applied bias of 1 V. ZnO@TiO₂ shows significantly larger photocurrent response as compared to bare ZnO NRs.*

Moreover, a comparison of the performance metrics of ZnO-based photodetectors [48-50] has been summarized in Table 1. Therefore, we believe that ZnO NRs coated with TiO₂ appear as one of the highly-sensitive self-powered ultraviolet photo detectors.

Table 1: Comparison of performance against other ZnO@TiO₂-based photodetectors.

Photo- detectors	R	D (Hz^{1/2}/W)	Response	ON/OFF	Ref.
	(mA/W)		Time	Ratio	
TiO ₂ /ZnO	514	3.2 x 10 ⁹	33.7/12 s	305	[48]
ZnO/TiO ₂	540	1.1 x 10 ¹⁰	9/20 s	388	[48]
Y-ZnO/TiO ₂ NWs-Au	27	6.2 x 10 ¹⁰	30 s	1786	[49]
ZnO-TiO ₂ /Si	~4500	-	-	1122	[50]
ZnO NRs	15	1.8 x 10 ¹⁴	< 30 s	375	This Work
ZnO@TiO ₂	90	6.4 x 10 ¹⁴	< 10s	416	

Conclusion

In summary, photosensitive devices based on bare ZnO NRs, as well as those coated with TiO₂ (ZnO@TiO₂), were successfully fabricated. SEM analysis and X-ray diffraction confirm the morphology and structural stability of as-prepared NRs. The optical band gap was measured and a comparative blue shift was observed in ZnO@TiO₂ NRs. First-principles DFT calculations at the GGA+U level of theory were performed to understand the geometry, electronic structure, and optical properties of both bare as well TiO₂ coated NRs. Our DFT calculations, coupled with suitable parameters, correctly predict the slight blue-shift in the band gap for the ZnO@TiO₂ NRs, as compared to the bare ones. In addition to the band-gap shift, strong enhancements in the photoconductivity were observed ZnO@TiO₂, as compared to bare ZnO NRs. With the UV light falling on the sample (“ON” state), there is a significant increase in photocurrent, while in the case of no incident UV light (“OFF” state), the dark current (I_{dark}), decreases in nanocomposites. Responsivity and detectivity of TiO₂ coated ZnO NRs based device found maximum in UV region

than bare ZnO NRs. ZnO@TiO₂ NRs show significant growth and decay in photocurrent for different wavelengths, leading to their increased photo-detection sensitivity and switching stability in the UV region, as compared to the bare ZnO NRs. Therefore, we believe that ZnO NRs coated with TiO₂ will prove to be very useful in fabrication of highly-sensitive self-powered ultraviolet photo detectors.

Acknowledgments

One of the authors (SP) acknowledges the Homi Bhabha Research Cum Teaching Fellowship (A.K.T.U.), Lucknow, India for providing financial support Through Teaching Assistantship. Authors sincerely thank Dr. Tejendra Dixit (Assistant Prof. IIIT kancheepuram) for his help during synthesis. One of the authors (SP) likes to thank Dr. Shivendra Pandey (Assistant Prof. NIT Silchar) for optical characterizations and his valuable suggestions in manuscript.

Compliance with ethical standards:

Conflict of interest: The authors declare that they do not have any conflict of interest.

Data availability statement –

The raw/processed data required to reproduce these findings cannot be shared at this time as the data also forms part of an ongoing study.

References

- [1] E. Monroy, F. O., and F. Calle, “Wide-bandgap semiconductor ultraviolet photodetectors,” *Semicond. Sci. Technol.*, vol. 18, no. 4, pp. R33–R51, Mar. 2003, doi: 10.1088/0268-1242/18/4/201.
- [2] K. Liu, M. Sakurai, M. Liao, and M. Aono, “Giant Improvement of the Performance of ZnO Nanowire Photodetectors by Au Nanoparticles,” *J. Phys. Chem. C*, vol. 114, no. 46, pp. 19835–19839, Nov. 2010, doi: 10.1021/jp108320j.
- [3] T. Srivastava, G. Bajpai, G. Rathore, S. W. Liu, S. Biring, and S. Sen, “Vanadium substitution: A simple and economic way to improve UV sensing in ZnO,” *Journal of Applied Physics*, vol. 123, no. 16, p. 161407, Apr. 2018, doi: 10.1063/1.5012877.

- [4] R. Khokhra, B. Bharti, H.-N. Lee, and R. Kumar, "Visible and UV photo-detection in ZnO nanostructured thin films via simple tuning of solution method," *Sci Rep*, vol. 7, no. 1, p. 15032, Nov. 2017, doi: 10.1038/s41598-017-15125-x.
- [5] A. J. Gimenez, J. M. Yáñez-Limón, and J. M. Seminario, "ZnO–Paper Based Photoconductive UV Sensor," *ACS Publications*, Dec. 13, 2010. <https://pubs.acs.org/doi/abs/10.1021/jp107812w> (accessed Jul. 21, 2021).
- [6] S. Hong et al., "Low-Temperature Rapid Fabrication of ZnO Nanowire UV Sensor Array by Laser-Induced Local Hydrothermal Growth," *Journal of Nanomaterials*, vol. 2013, p. e246328, Jul. 2013, doi: 10.1155/2013/246328.
- [7] X. Bai, L. Wang, R. Zong, Y. Lv, Y. Sun, and Y. Zhu, "Performance Enhancement of ZnO Photocatalyst via Synergic Effect of Surface Oxygen Defect and Graphene Hybridization," *Langmuir*, vol. 29, no. 9, pp. 3097–3105, Mar. 2013, doi: 10.1021/la4001768.
- [8] V. Mishra et al., "Diffuse reflectance spectroscopy: An effective tool to probe the defect states in wide band gap semiconducting materials," *Materials Science in Semiconductor Processing*, vol. 86, pp. 151–156, Nov. 2018, doi: 10.1016/j.mssp.2018.06.025.
- [9] C. Zhao et al., "Low temperature growth of hybrid ZnO/TiO₂ nano-sculptured foxtail-structures for dye-sensitized solar cells," *RSC Adv.*, vol. 4, no. 105, pp. 61153–61159, Nov. 2014, doi: 10.1039/C4RA11881B.
- [10] L. Wang et al., "ZnO@TiO₂ heterostructure arrays/carbon cloth by charge redistribution enhances performance in flexible anode for Li ion batteries," *Electrochimica Acta*, vol. 295, pp. 107–112, Feb. 2019, doi: 10.1016/j.electacta.2018.10.146.
- [11] U. Diebold, "The surface science of titanium dioxide," *Surface Science Reports*, vol. 48, no. 5, pp. 53–229, Jan. 2003, doi: 10.1016/S0167-5729(02)00100-0.
- [12] U. Diebold, J. F. Anderson, K.-O. Ng, and D. Vanderbilt, "Evidence for the Tunneling Site on Transition-Metal Oxides: TiO₂(110)," *Phys. Rev. Lett.*, vol. 77, no. 7, pp. 1322–1325, Aug. 1996, doi: 10.1103/PhysRevLett.77.1322.
- [13] V. Mishra et al., "Investigation of temperature-dependent optical properties of TiO₂ using diffuse reflectance spectroscopy," *SN Appl. Sci.*, vol. 1, no. 3, p. 241, Feb. 2019, doi: 10.1007/s42452-019-0253-6.

- [14] Y. Li, F. D. Valle, M. Simonnet, I. Yamada, and J.-J. Delaunay, "High-performance UV detector made of ultra-long ZnO bridging nanowires," *Nanotechnology*, vol. 20, no. 4, p. 045501, Dec. 2008, doi: 10.1088/0957-4484/20/4/045501.
- [15] J. Zhou et al., "Gigantic enhancement in response and reset time of ZnO UV nanosensor by utilizing Schottky contact and surface functionalization," *Appl. Phys. Lett.*, vol. 94, no. 19, p. 191103, May 2009, doi: 10.1063/1.3133358.
- [16] J. Agrawal, T. Dixit, I. A. Palani, and V. Singh, "Highly Visible-Blind ZnO Photodetector by Customizing Nanostructures With Controlled Defects," *IEEE Photonics Technology Letters*, vol. 32, no. 22, pp. 1439–1442, Nov. 2020, doi: 10.1109/LPT.2020.3031732.
- [17] T. Dixit, M. Shukla, I. A. Palani, and V. Singh, "Insight of dipole surface plasmon mediated optoelectronic property tuning of ZnO thin films using Au," *Optical Materials*, vol. 62, pp. 673–679, Dec. 2016, doi: 10.1016/j.optmat.2016.10.053.
- [18] J. Agrawal, T. Dixit, I. A. Palani, and V. Singh, "Electron Depleted ZnO Nanowalls-Based Broadband Photodetector," *IEEE Photonics Technology Letters*, vol. 31, no. 20, pp. 1639–1642, Oct. 2019, doi: 10.1109/LPT.2019.2940881.
- [19] T. Dixit, J. Agrawal, S. V. Solanke, K. L. Ganapathi, M. S. R. Rao, and V. Singh, "ZnO/Au/ZnO Configuration for High Performance Multiband UV Photo-Detection," *IEEE Sensors Letters*, vol. 3, no. 9, pp. 1–4, Sep. 2019, doi: 10.1109/LESENS.2019.2940764.
- [20] M. S. Alam, U. Manzoor, M. Mujahid, and A. S. Bhatti, "Highly Responsive UV Light Sensors Using Mg-Doped ZnO Nanoparticles," *Journal of Sensors*, vol. 2016, p. e8296936, Mar. 2016, doi: 10.1155/2016/8296936.
- [21] I.-K. Jeong, S. Lee, S.-Y. Jeong, C. J. Won, N. Hur, and A. Llobet, "Structural evolution across the insulator-metal transition in oxygen-deficient BaTiO₃ studied using neutron total scattering and Rietveld analysis," *Phys. Rev. B*, vol. 84, no. 6, p. 064125, Aug. 2011, doi: 10.1103/PhysRevB.84.064125.
- [22] K. Chongsri and W. Pecharapa, "UV photodetector based on Al-doped ZnO nanocrystalline sol-gel derived thin films," *Energy Procedia*, vol. 56, no. C, pp. 554–559, 2014, doi: 10.1016/j.egypro.2014.07.192.
- [23] K. Manjunath and V. S. Souza and T. Ramakrishnappa and G. Nagaraju and J. D. Scholten and J. Dupont, "Heterojunction CuO-TiO₂ nanocomposite synthesis for significant photocatalytic hydrogen production," *Materials Research Express*, vol. 3, no. 11, p. 115904, 2016.

- [24] N. Wang, C. Sun, Y. Zhao, S. Zhou, P. Chen, and L. Jiang, "Fabrication of three-dimensional ZnO/TiO₂ heteroarchitectures via a solution process," *J. Mater. Chem.*, vol. 18, no. 33, pp. 3909–3911, Aug. 2008, doi: 10.1039/B809385G.
- [25] H. von Wenckstern et al., "Lateral homogeneity of Schottky contacts on n-type ZnO," *Appl. Phys. Lett.*, vol. 84, no. 1, pp. 79–81, Jan. 2004, doi: 10.1063/1.1638898.
- [26] K. Yoshino et al., "Electrical and optical characterization of n-type ZnO thin films," *physica status solidi (c)*, vol. n/a, no. 2, pp. 626–630, 2003, doi: 10.1002/pssc.200306187.
- [27] Y.-J. Lin, J.-S. Huang, H.-C. Chang, C. Y. Chuang, and M.-H. Lin, "Effects of the addition of graphene on the defect-related photoluminescent and electrical properties of n-type ZnO thin films," *Journal of Luminescence*, vol. 242, p. 118599, Feb. 2022, doi: 10.1016/j.jlumin.2021.118599.
- [28] J. Bao et al., "Photoinduced oxygen release and persistent photoconductivity in ZnO nanowires," *Nanoscale Research Letters*, vol. 6, no. 1, p. 404, May 2011, doi: 10.1186/1556-276X-6-404.
- [29] R. J. Collins and D. G. Thomas, "Photoconduction and Surface Effects with Zinc Oxide Crystals," *Phys. Rev.*, vol. 112, no. 2, pp. 388–395, Oct. 1958, doi: 10.1103/PhysRev.112.388.
- [30] P. Hohenberg and W. Kohn, "Inhomogeneous Electron Gas," *Phys. Rev.*, vol. 136, no. 3B, pp. B864–B871, Nov. 1964, doi: 10.1103/PhysRev.136.B864.
- [31] W. Kohn and L. J. Sham, "Self-Consistent Equations Including Exchange and Correlation Effects," *Phys. Rev.*, vol. 140, no. 4A, pp. A1133–A1138, Nov. 1965, doi: 10.1103/PhysRev.140.A1133.
- [32] G. Kresse, J. Hafner, "Norm-conserving and ultrasoft pseudopotentials for first-row and transition elements," *J. Phys.: Condens. Matter* 6 8245, 1994. <http://iopscience.iop.org/article/10.1088/0953-8984/6/40/015/meta;jsessionid=A58F298FB63E570E0FD15C605A1A55E5.c4.iopscience.cld.iop.org> (accessed Feb. 13, 2017).
- [33] G. Kresse, J. Furthmüller, "Efficient iterative schemes for ab initio total-energy calculations using a plane-wave basis set," *Phys. Rev. B* 54, 11169, Oct. 15, 1996. <http://journals.aps.org/prb/abstract/10.1103/PhysRevB.54.11169> (accessed Feb. 13, 2017).

- [34] K. Yang, Y. Dai, B. Huang, and Y. P. Feng, “First-principles GGA+U study of the different conducting properties in pentavalent-ion-doped anatase and rutile TiO₂,” *J. Phys. D: Appl. Phys.*, vol. 47, no. 27, p. 275101, Jun. 2014, doi: 10.1088/0022-3727/47/27/275101.
- [35] A. Rubio-Ponce, A. Conde-Gallardo, and D. Olgún, “First-principles study of anatase and rutile TiO₂ doped with Eu ions: A comparison of GGA and LDA+U calculations,” *Phys. Rev. B*, vol. 78, no. 3, p. 035107, Jul. 2008, doi: 10.1103/PhysRevB.78.035107.
- [36] H. Ehrenreich and M. H. Cohen, “Self-Consistent Field Approach to the Many-Electron Problem,” *Phys. Rev.*, vol. 115, no. 4, pp. 786–790, Aug. 1959, doi: 10.1103/PhysRev.115.786.
- [37] S. Panigrahi and D. Basak, “Core-shell TiO₂@ZnO nanorods for efficient ultraviolet photodetection,” *Nanoscale*, vol. 3, no. 5, pp. 2336–2341, May 2011, doi: 10.1039/C1NR10064E.
- [38] Z. Zhang, Y. Yuan, Y. Fang, L. Liang, H. Ding, and L. Jin, “Preparation of photocatalytic nano-ZnO/TiO₂ film and application for determination of chemical oxygen demand,” *Talanta*, vol. 73, no. 3, pp. 523–528, Sep. 2007, doi: 10.1016/j.talanta.2007.04.011.
- [39] J. Qiu, W. Yu, X. Gao, and X. Li, “Sol-gel assisted ZnO nanorod array template to synthesize TiO₂ nanotube arrays,” *Nanotechnology*, vol. 17, no. 18, pp. 4695–4698, Aug. 2006, doi: 10.1088/0957-4484/17/18/028.
- [40] T. Takagahara and K. Takeda, “Theory of the quantum confinement effect on excitons in quantum dots of indirect-gap materials,” *Phys. Rev. B*, vol. 46, no. 23, pp. 15578–15581, Dec. 1992, doi: 10.1103/PhysRevB.46.15578.
- [41] J. von Behren, T. van Buuren, M. Zacharias, E. H. Chimowitz, and P. M. Fauchet, “Quantum confinement in nanoscale silicon: The correlation of size with bandgap and luminescence,” *Solid State Communications*, vol. 105, no. 5, pp. 317–322, Feb. 1998, doi: 10.1016/S0038-1098(97)10099-0.
- [42] S. Pandey, A. Shukla, and A. Tripathi, “Elucidating the influence of native defects on electrical and optical properties in semiconducting oxides: An experimental and theoretical investigation,” *Computational Materials Science*, p. 111037, Nov. 2021, doi: 10.1016/j.commatsci.2021.111037.
- [43] P. Singh et al., “Role of H-bond along with oxygen and zinc vacancies in the enhancement of ferromagnetic behavior of ZnO films: An experimental and first principle-based study,”

Journal of Alloys and Compounds, vol. 889, p. 161663, Dec. 2021, doi: 10.1016/j.jallcom.2021.161663.

- [44] P. P. Das, S. Samanta, L. Wang, J. Kim, T. Vogt, P. S. Devi, and Y. Lee, Redistribution of native defects and photoconductivity in ZnO under pressure, RSC Adv., vol. 9, p. 4303-4313, feb. 2019, doi: 10.1039/C8RA10219H.
- [45] S. Pandey, A. Shukla, A. Tripathi, Effect of pressure on electrical and optical properties of metal doped TiO₂, Opt. Mater. 133 (2022) 112875. <https://doi.org/10.1016/j.optmat.2022.112875>.
- [46] A. Sumanth, V. Mishra, P. Pandey, M.S.R. Rao, T. Dixit, Investigations into the Role of Native Defects on Photovoltaic and Spintronic Properties in Copper Oxide, IEEE Trans. Nanotechnol. vol. 21, p. 522-527, Sept. 2022. <https://doi.org/10.1109/TNANO.2022.3204587>.
- [47] S. Arige, V. Mishra, M. Miryala, M.S.R. Rao, T. Dixit, Plasmon-coupled sub-bandgap photoluminescence enhancement in ultra-wide bandgap CuO through hot-hole transfer, Opt. Mater. vol. 134, p. 113149, Dec. 2022, <https://doi.org/10.1016/j.optmat.2022.113149>.
- [48] M. Zhou, B. Wu, X. Zhang, S. Cao, P. Ma, K. Wang, Z. Fan, M. Su, Preparation and UV photoelectric properties of aligned ZnO-TiO₂ and TiO₂-ZnO core-shell structured heterojunction nanotubes, ACS Appl. Mater. Interfaces vol. 12, p. 38490–38498, July 2020, doi: 10.1021/acsami.0c03550.
- [49] C. Hsu, H. Wu, C. Fang, S. Chang, Solution-Processed UV and Visible Photodetectors Based on Y-Doped ZnO Nanowires with TiO₂ Nanosheets and Au Nanoparticles, ACS Appl. Energy Mater. vol. 1, p. 2087–2095, April 2018 doi: 10.1021/acsaem.8b00180.
- [50] M. Monshipouri, S. Molavi, A. Mosaddegh, M. Sasar, Y. Abdi, Enhancement of responsivity and sensitivity of p-Silicon/n-Zinc oxide-based photodetector using titanium dioxide nanoparticles, IEEE Transactions on Nanotechnology vol. 19, p. 744–748, sept. 2020, doi: 10.1109/TNANO.2020.3022662.